Int. J. Electrochem. Sci., 10 **(2015)** 9456 - 9465

International Journal of
ELECTROCHEMICAL
SCIENCE
www.electrochemsci.org

Facial In-situ Synthesis of MnO_2/PPy Composite for Supercapacitor

Liyang Yuan, Chuanyun Wan[*]*, Liangliang Zhao*

School of Chemical and Environmental Engineering, Shanghai Institute of Technology, Shanghai 200235, China
[*]E-mail: cywan@sit.edu.cn

Received: 5 August 2015 / *Accepted:* 31 August 2015 / *Published:* 30 September 2015

Manganese dioxide/polypyrrole composites as supercapacitor electrode materials are successfully prepared by in situ chemical oxidative polymerization. X-ray diffraction spectroscopy measurement(XRD)，Fourier transform infrared spectroscopy (FTIR)， Canning electron microscope (SEM) and transmission electron microscope (TEM) reveal that MnO_2 nanoparticles are incorporated in PPy matrix. Cyclic voltammetry (CV) indicates that the combination of MnO_2 and PPy enhances the capability of the composite and the largest specific capacitance, 205F g^{-1}, is obtained when the content of MnO_2 in composite is ca.30%. Electrochemical impedance spectroscopy (EIS) measurements prove that 30.5%MnO_2/PPy composite electrodes own the smallest charge transfer resistance and the chronopotentiometry test indicates that MnO_2/PPy composite have an ideal capacitive behavior and an excellent cyclibility. The excellent electrochemical performances of MnO_2/PPy composite suggest that in-situ chemical oxidation polymerization is an effective method to obtain MnO_2/PPy composite for supercapacitors.

Keywords: polypyrrole; manganese dioxide; electrochemical supercapacitor

1. INTRODUCTION

As a new energy storage device, supercapacitors (ECs) have aroused great attention owing to its superior power delivery and cycling life compared to those of rechargeable batteries and superior density delivery compared to those of conventional electrolytic capacitors [1]. Then ECs offer a promising approach to meet the increasing power demands of energy storage systems in computer power backup, medical equipment, load leveling, electrical vehicles, space crafts and etc. [2-6]. Since the performances of supercapacitors are mainly determined by electrode material, it is important to develop electrode materials. Based on the electrochemical behavior and charge/energy storage mechanisms, the supercapacitors are classified into electrical double layer capacitors and pseudo-capacitors. Typical electrode materials for EDLCs include high surface area carbon, which stores

energy in a double layer formed on the surface，while, in the case of the pseudo-capacitors, most electrode materials which consist of metal oxides or conducting poymers transfer faradic charges between an electrolyte and electrode [7].Composite materials based on metal oxides/conducting polymers have attracted tremendous attentions for their higher energy/power capability [8-10].

Among different metal oxides, manganese dioxide as supercapacitor electrodes has been extensively studied due to its high theoretical capacitance (1370F g^{-1}), low cost, low toxicity and resource abundance [9-11]. Manganese dioxide offers high pseudocapacitance through fast and reversible redox reactions near the surface of active materials[12]. Nevertheless, MnO_2 has a poor electronic/ionic conductivity which often results in low utilization of materials and capacitance loss seriously at large current condition, limiting the practical applications of MnO_2 in supercapacitors. Therefore, overcoming these disadvantages of MnO_2 electrode material for its commercial applications is an imperative task[13]. Polypyrrole (PPy) is known as one of the most frequently investigated important conducting polymers due to its high conductivity, easy-preparation, good environmental stability and no toxicity [14, 15]. It is expected that the combination of PPy and manganese dioxide will produce synergetic effect. For example, Dong et al[16] prepared manganese oxide (MnO_2)/doped-polypyrrole by chemical oxidative polymerization. It is observed that the dispersed MnO_2 adhered to PPy chains increased the specific surface area of the nanocomposite and retarded the structural deterioration of PPy backbones during charge-discharge cycling process[16]. Due to the synergic effect between MnO_2 core and PPy shell, the MnO_2@PPy coaxial nanotubes possess better rater capability, larger specific capacitance and good capacitance retention[17]. Bahloul[18] prepared PPy-covered MnO_2 by electrodepositing PPy on MnO_2 particles and found that the presence of PPy improves the electrochemical performance of the composite material electrode and increases the specific capacitance. It is evident that the MnO_2/PPy composites own a better capacitance performance than pure MnO_2 or pure PPy. Even in-situ method was reported in few references[16,19], the current reported combination processes for MnO_2/PPy composites are often operated step by step, which is complex and time-waste [17, 18, 20-22].

In this paper, we investigated one-step in-situ chemical redox method to synthesize nanostructured MnO_2/PPy composites for supercapacitor, aiming to achieve a composite electrode with optimized electrochemical properties. X-ray diffraction (XRD), Scanning electron microscope (SEM), transmission electron microscope (TEM), Brunauer Emmett Teller (BET) measurements and Fourier transform infrared spectroscopy (FTIR) were used to investigate the physical properties. Cyclic voltammetry (CV), chronopotentiometry and electrochemical impedance spectrum (EIS) were employed to characterize their capacitance performances.

2. EXPERIMENTAL

2.1 Preparation of MnO_2/ PPy composites

Pyrrole (Py) monomer, ferric chloride hexahydrate ($FeCl_3$•$6H_2O$), potassium permanganate ($KMnO_4$), manganese sulfate hydrate ($MnSO_4$•H_2O), anhydrous ethanol are analytical grade. Before

use, pyrrole is distilled under reduced pressure and stored at a temperature below 4℃, other reagents are used as received without further treatment. In the synthesis of MnO_2/PPy composites, $KMnO_4$ is mainly aimed for the oxidation of Mn^{2+} while $FeCl_3$ is mainly for the oxidation of pyrrole. The typical synthesis process was carried out as follows: Firstly, some amounts of $MnSO_4 \cdot H_2O$ and pyrrole monomer are co-dissolved in 200 mL distilled water and stirred continuously for ten minutes to form a homogeneous solution. Secondly, metrological amount of $KMnO_4$ (the molar ratio to $MnSO_4 \cdot H_2O$ was controlled to be 2:3) was added to the solution under stirring condition. Subsequently, 0.9mol/L ferric chloride solution (the molar ratio to pyrrole was controlled to be 3:1) dropped slowly into the above mixture. The polymerization was made to continue under constant stirring condition for 6 h. After polymerization, it was filtered and the black solid particles are collected and washed with deionized water. Finally, the residue was dried at 80 ℃ in vacuum oven for 12h to get the PPy/MnO_2 composites.

For comparison, pure PPy was prepared by slowly adding 0.9mol/L ferric chloride solution into pyrrole solution at 0-2℃ for 6h under stirring condition. MnO_2 was prepared by slowly adding $KMnO_4$ solution to the 200 mL 0.03mol L^{-1} $MnSO_4 \cdot H_2O$ solution and stirring for 6h.

2.2. Structure Characterization

Morphologies of composites were characterized by scanning electron microscopy (SEM, Hitachi S-3400N, Japan) and transmission electron microscopy (TEM, Hitachi600, Japan). Chemical composition analysis of composite were investigated by energy dispersive spectroscopy(EDS, Hitachi S-3400N, Japan) and a Thermo scientific Nicolet iz10 IR spectrophotometer(FTIR) using KBr pressed disks. The crystal structure measurement of the samples was performed on an X-Ray Diffractometer (X'pert Pro).

2.3 Electrochemical measurements

Testing electrodes for electrochemical capacitors were prepared by mixing 65 wt. % prepared samples with 25 wt. % super-P and 10 wt. % Polyvinylidene Fluoride (PVDF) binder to form slurry. A little ethanol was added to the mixtures to make them more homogeneous. The slurry was pressed onto nickel foam current collectors with a blade to fabricate electrodes and then drying the formed electrodes at 50 °C for about 12 h. The typical loading of electrode material was ca. 10 mg cm^{-2}.

The electrochemical performances were conducted in a three-electrode electrolytic cell. A platinum electrode and a saturated calomel electrode were used as counter and reference electrodes, respectively. The working electrolyte was 1mol/L Na_2SO_4 solution. Cyclic voltammetry (CV), chronopotentiometry and Electrochemical impedance spectroscopies (EIS) were performed using an Autolab electrochemical workstation. EIS were taken at open circuit potential (OCP) over the frequency range 10 kHz to 10 m Hz with a potential amplitude of 5 mV. All the experiments were performed at the room temperature.

3. RESULTS AND DISCUSSION

3.1 Structure characterization

X-ray diffraction patterns of PPy, MnO_2, MnO_2/PPy composite particles are shown in Fig. 1. The MnO_2 sample exhibits weak and broad peaks distinguishable at 2θ= 37.6 and 66.4°.

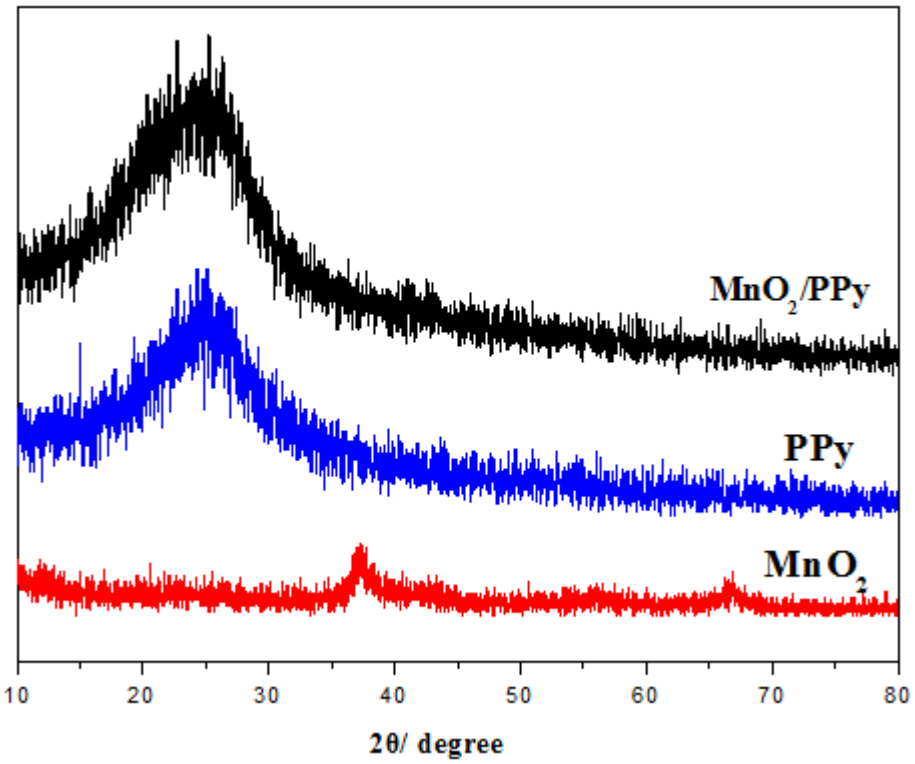

Figure 1. XRD patterns of the PPy, MnO_2, PPy/MnO_2 composite particles

Although these are in sufficient to illustrate a certain crystallographic form, it does indicate the formed MnO_2 is in poorly crystalline phase and is a mixture of poorly crystallized oxides and amorphous oxide. The broad weak at 2θ value from 15° to 30° appeared in PPy and MnO_2/PPy composite is the characteristic peak of the amorphous PPy, indicating the presence of PPy[23]. No evident peaks for MnO_2 were observed in XRD patterns of MnO_2/PPy composite. This could be a part of distortion in crystal structure of MnO_2 and also may be that MnO_2 particles were covered by PPy coating.

FT-IR spectra of the prepared PPy, MnO_2 and MnO_2/PPy composite are shown in Fig.2. For pure MnO_2 sample, the peak around 1636cm^{-1} band was normally attributed to O–H bending vibrations and the broad band between 400-700cm^{-1} to the Mn-O bond[24, 25]. For the MnO_2/PPy composite and pure PPy, all characteristic bands at 1550, 1304, 1160, 1044 and 780 cm^{-1} are corresponding to PPy phase, indicating the formation of polypyrrole. The band at 1550cm^{-1} is attributed to the pyrrole ring vibration[26, 27]. The bands located at 1304 and 1160cm^{-1} are ascribed to the C- H in-plane deformation and the C- N stretching vibrations[28]. The other bands at 1044cm^{-1}

reflected N-H in-plane deformation vibration of the doped PPy[29]. Observing the IR spectra of PPy and MnO_2/PPy composite carefully, the intensity and position of PPy peaks were influenced by incorporation of MnO_2 in the MnO2/PPy composite, although the two spectra of MnO_2/PPy composite and PPy were very similar., the absence of IR spectra about MnO_2 in MnO_2/PPy composite indicated that MnO_2 was embedded in PPy matrix, which is in accordance with the result of the XRD measurement.

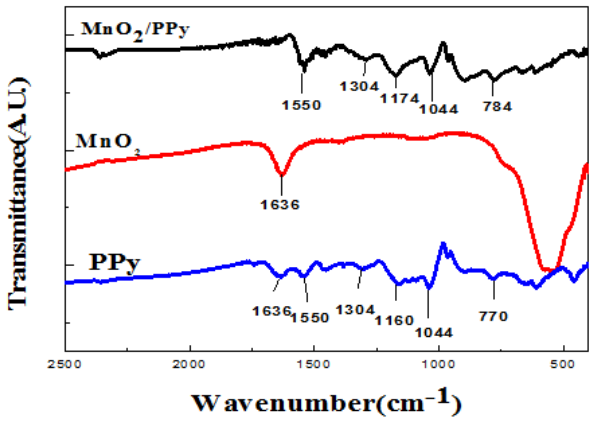

Figure 2. FT-IR transmittance spectra of the PPy, MnO_2 and MnO_2/PPy samples

The morphologies and structures of the samples are further examined by scanning electron microscope (SEM) and transmission electron microscope (TEM). Fig.3 shows the SEM and TEM images of MnO_2, PPy and typical MnO_2/PPy particles.

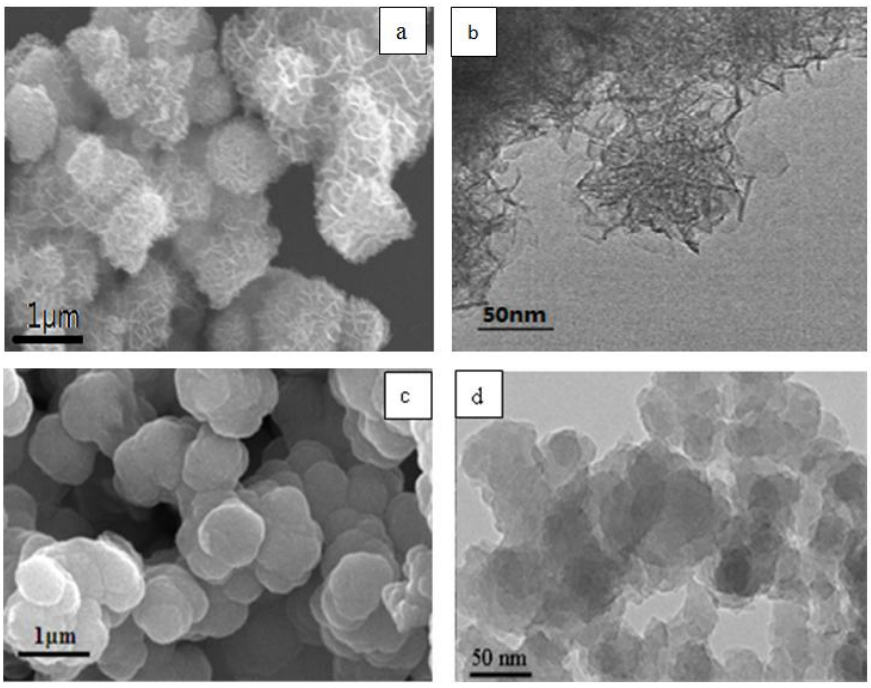

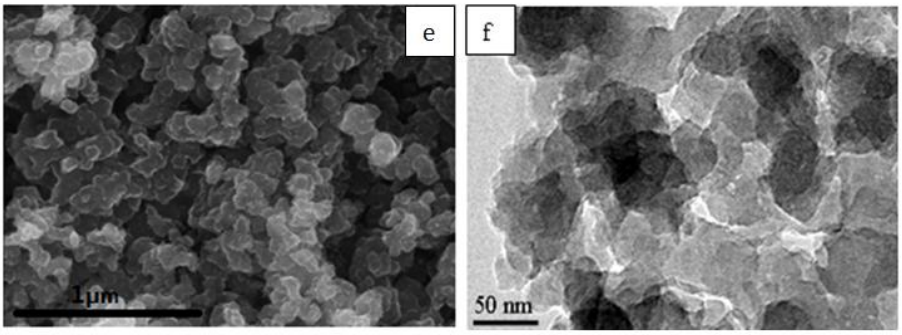

Figure 3. SEM (left) and TEM (right) images of MnO_2 (a, b), PPy (c, d) and MnO_2/PPy(e, f).

The pure MnO_2 particles were semispherical with coarse surface morphology, while the PPy polymer exhibits an agglomeration of semispherical particles. The size of MnO_2/PPy particles is much smaller than MnO_2 or PPy sample. Compared with MnO_2 or PPy, a distinguished black core in MnO_2/PPy samples can be seen from the TEM image, which indicates that MnO_2 particles are incorporated into PPy matrix. This is the reason why MnO_2 can't be apparently detected in XRD patterns and FT-IR transmittance spectra. Even the EDS measurement still detected small amount of Mn elements, the above results reveals that large amount of Mn^{2+} ion are oxidized by MnO_4^+ before pyrrole polymerization.

3.2 Electrochemical performances

To identify the oxidation and reduction potentials and the reciprocally effect of PPy on the electrochemical performance of MnO_2, cyclic voltammograms (CVs) of PPy, MnO_2 and MnO_2/PPy composites electrode at 2 mV s^{-1} in 1 mol L^{-1} Na_2SO_4 electrolyte are shown in Fig. 4.

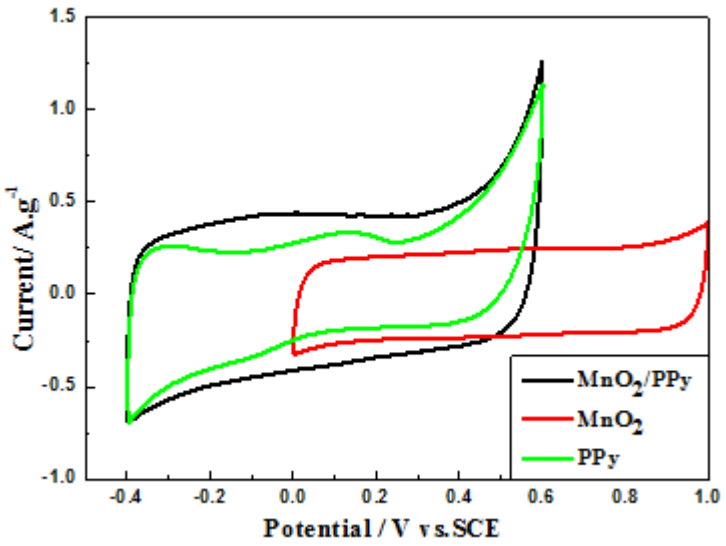

Figure 4. CV curves of the MnO_2, PPy and MnO_2/PPy electrodes at scan rate of 2mV s^{-1}

It is seen that the MnO_2 electrode and the MnO_2/PPy electrode exhibit capacitive characteristics in different potential ranges. The potential window of the MnO_2/PPy electrode is from -0.4V to 0.6V vs. SCE as the same as the PPy electrode, while the window of the MnO_2 electrode is between 0.0V and 1.0V vs. SCE, this result apparently indicates that MnO_2 particles are mainly embedded in PPy matrix. The increase of response current density for MnO_2/PPy electrode may be attributed to the decrease of the internal resistance since high conductive PPy chains are adhered to the low conductive MnO_2 particles.

Fig.5a shows the specific capacitance of MnO_2/PPy electrodes with different MnO_2 content. With the increase of MnO_2 content, the electrode specific capacitance initially increased and reaches its maximum value of 205 F g^{-1} when it comes to 30.5%, and then decreased. The result indicates that an effective synergistic function of PPy and MnO_2 may be occurred in a reasonable condition. For this in-situ method, the optimized MnO_2/PPy composite with maximum capacity is containing ca.30% MnO_2. Fig.5b shows electrochemical impedance spectra in the form of Nyquist plots for the pure MnO_2, pure PPy and MnO_2/PPy composites electrodes, where Z' and Z'' are the real and imaginary parts of the impedance, respectively. The equivalent circuit diagram used for the fitting of the EIS is displayed in the inset. In the impedance spectra, there is a semi-circle feature at the high frequency region followed by a line at the low frequency region. The results indicate the electrode process is controlled by electrochemical reaction at high frequencies and by mass transfer at low frequencies [8,9,31,32]. There is no evident change in the solution resistance (R_s) for all electrodes, indicating that the solution resistance mainly results from the electrolytes used. The diameter of the semicircles of electrodes is associated with the charge transfer resistance (R_{ct}). Compared these electrodes, the MnO_2/PPy composite electrode containing ca. 30% MnO_2 shows the smallest charge transfer resistance, indicating its best conductivity. This result supports its best capacitance in Fig.5a.

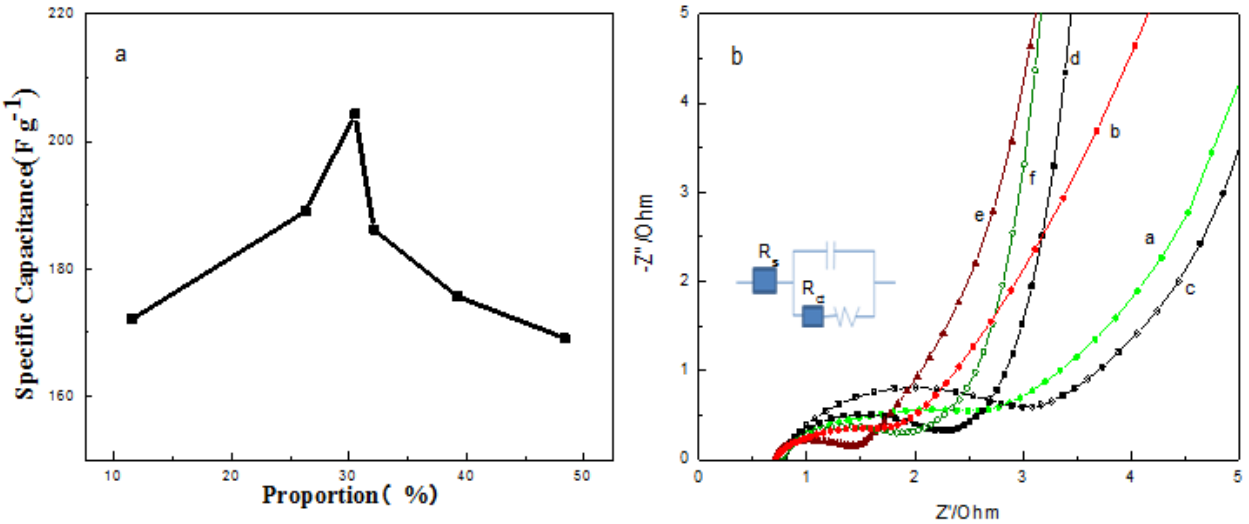

Figure 5. Specific capacitance of MnO_2/PPy composite electrodes with different MnO_2 content（a） and Nyquist impedance plots(b) of MnO_2(a), PPy(b), and PPy/MnO_2 composites electrodes with MnO_2 content of 11.3%(c), 25.4%(d), 30.5%(e), 48.4%(f).

To extensively understand the electrochemical properties of the MnO_2/PPy composite electrodes, the charge-discharge behavior was examined by Chronopotentiometry.

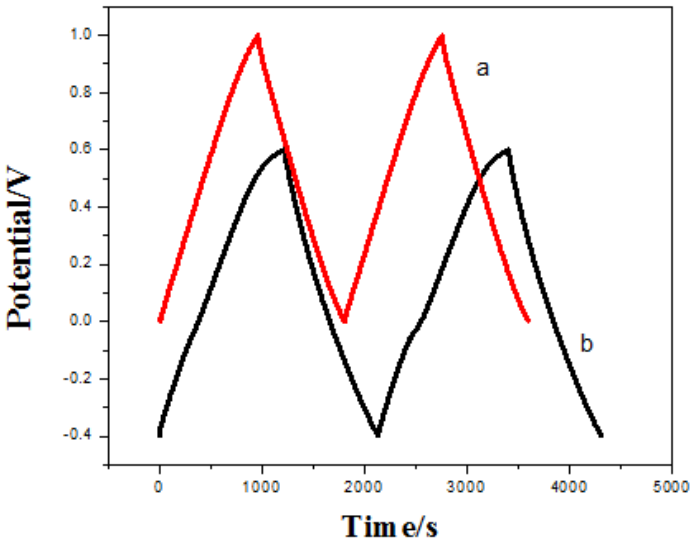

Figure 6. Charge-discharge curves of (a) MnO_2 and (b) PPy/MnO_2 composites at current density of 0.1A g^{-1}

Fig.6 shows the charge/discharge curves for both the MnO_2 and MnO_2/PPy electrodes at current density of 0.1A·g^{-1} in a potential range of 0~1.0 V and -0.4~0.6V in 1mol L^{-1} Na_2SO_4 electrolyte, respectively. The both curves are approximately symmetric and linear for both charge and discharge portions, indicating that the electrodes have good capacitive behaviors. The results manifest that the MnO_2/PPy composite electrode enhances the capacitive performance of pure PPy and MnO_2 electrode.

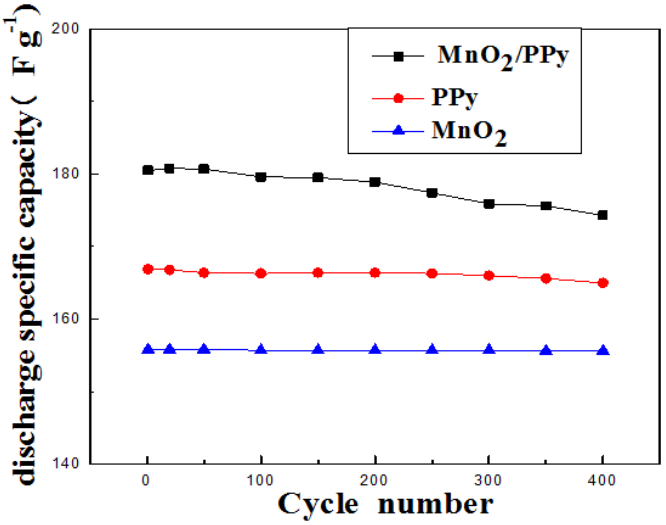

Figure 7. Cycle behavior of PPy, MnO_2 and MnO_2/PPy electrodes by Chronopotentiometry.

The life test was conducted by Chronopotentiometry（Fig.7）. After 400 cycles, the capacitance retention of MnO_2/PPy is 96.5%, similar to the value of PPy electrode (95.7%) and MnO_2 electrode (96.8%). The reasonable stability implies that the MnO_2/PPy composite can be a good candidate for supercapacitor electrode material.

4. CONCLUSIONS

MnO_2/PPy composite particle composites are successfully prepared through in-situ chemical oxidative polymerization method. The physical characterizations of the synthesized composite nanoparticles are performed by XRD, FTIR, SEM and TEM. The results indicate that MnO_2 is mainly cladded by PPy layer and there is an interaction between MnO_2 and PPy. The electrochemical properties are studied by CV, AC and constant charge-discharge methods. The results suggest that the capacitive performances of MnO_2/PPy composites are improved compared with pure MnO_2 electrode and pure PPy electrode. For this method, the optimized MnO_2/PPy composite contains ca.30% MnO_2, owning the capacitance of 205 F g^{-1} at 2mV s^{-1} in 1mol L^{-1} Na_2SO_4. The good conductivity and good cyclic stability suggested that they might can be used as an electrode material in electrochemical capacitor.

References

1. H. Sayahi, M.A. Kiani, S.H. Kazemi. *J Solid State Electrochem*, 18(2014) 535
2. J. R. Miller, P. Simon. *Science*, 321(2008) 651
3. A. K. Arof, N. E. A. Shuhaimi, N. A. Alias, M. Z. Kufian, S. R. Majid. *J Solid State Electrochem.* 14(2010) 2145
4. P. Iora, J. Thangavelautham. *Int. J. Hydro. Energy*, 37(2012) 17191.
5. C. Heymans, S. Walker, S. B. Young, M. Fowler. *Energy Policy*, 71(2014) 22
6. O. Kraa, M. Becherif, M.Y. Ayad, R. Saadi, M. Bahri, A. Aboubou, I. Tegani. *Energy Procedia*, 50(2014) 194
7. M. Kim, Y. Hwang, J. Kim. *Phys. Chem. Chem. Phys.*, 16(2014) 351
8. X. Li, Y.J. Wu, F. Zheng. M. Ling, F.H. Lu. *Solid State Commun.*197(2014) 57
9. M. Jin, G.Y. Han, Y.Z. Chang, H. Zhao, H.Y. Zhang. *Electrochimica Acta*, 56(2011) 9838
10. L.J. Sun, X.X. Liu, K. K.T. Lau, L. Chen, W.M. Gu. *Electrochim. Acta* 53 (2008) 3036
11. C.Y. Wan, M. Cheng, Q.S. Zhang, N.Q. Jia. *Powder Techn.* 235(2013) 706
12. C.Y.Wan, L.Y. Yuan, H.Y. Shen. *Int. J. Electrochem. Sci.*, 9 **(**2014**)** 4024
13. Y.Q. Zhang, Y. Mo. *Electrochim. Acta*, 142(2014) 76
14. K.Q. Ding, H.T. Jia, S.Y. Wei, Z.H. Guo. *Ind. Eng. Chem. Res.*, 50(2011) 7077
15. L.F. Yang, Z. Shi, W.H. Yang. *Electrochimica Acta*, 153 (2015) 76
16. Z.H. Dong, Y.L. Wei, W. Shi, G.A. Zhang. *Mater. Chem. Phys.* 131 (2011) 529
17. W. Yao, H. Zhou, Y. Lu, *J. Power Sources*, 241(2013) 359
18. A. Bahloul, B. Nessark, E. Briot, H. Groult, A. Mauger, K. Zaghib, C.M. Julien. *J. Power Sources*, 240(2013) 267
19. S. Grover, S. Shekhar, R. K. Sharma, G. Singh. *Electrochim. Acta*, 116 (2014) 137
20. J. Li, T.L.Que, J.B. Huang. *Mater. Res. Bull.*, 48 (2013) 747
21. L.J. Han, P.Y. Tang, L. Zhang. *Nano Energy*, 7(2014) 42

22. J. Li, L. Cui, X.G. Zhang. *Appl. Surf. Sci.*, 256(2010): 4339
23. S.B. Wang, G.Q. Shi. *Mater. Chem. Phys.* 102(2007) 255
24. H.Y. Chu, Q.Y. Lai, L. Wang, J.F. Lu, Y. Zhao. *Ionics*, 16(2010) 233
25. A.B. Yuan, Q.L. Zhang. *Electrochem Commun.*, 2006, 8(2006) 1173
26. [D.S. Kumar, K. Nakamura, S. Nishiyama, S. Ishii, H. Noguchi, K. Kashiwagi, Y. Yoshida. *J. Appl. Phys*. 93(2003) 2705
27. T.K. Vishnuvardhan, V.R. Kulkarni, C. Basavaraja, S. C. Raghavendra. *Bull. Mater. Sci.*, 29(2006) 77
28. J. Jang, J. H. Oh. *Adv. Funct. Mater.*, 15(2005): 494
29. Y. C. Jung, N. G. Sahoo, J. W. Cho. *Macromol. Rapid Commun.*, 27 (2006) 126
30. R.R. Muthuchudarkodi, C. Vedhi. Appl. Nanosci., 5(2015) 481
31. N. Y. Li, D. Shan, H.G. Xue. *Eur. Polymer J.*, 43(2007) 2532
32. P. Sen, A. De, A. D. Chowdhury, S.K. Bandyopadhyay, N. Agnihotri, M. Mukherjee. *Electrochim. Acta*, 108(2013) 265